THE JOURNAL OF BIOLOGICAL CHEMISTRY
Vol. 279, No. 25, Issue of June 18, pp. 26654–26665, 2004
Printed in U.S.A.

Identification of a Novel A-kinase Anchoring Protein 18 Isoform and Evidence for Its Role in the Vasopressin-induced Aquaporin-2 Shuttle in Renal Principal Cells*

Received for publication, November 24, 2003, and in revised form, March 11, 2004
Published, JBC Papers in Press, March 22, 2004, DOI 10.1074/jbc.M312835200

Volker Henn‡, Bayram Edemir‡, Eduard Stefan‡, Burkhard Wiesner‡, Dorothea Lorenz‡, Franziska Theilig§, Roland Schmitt§, Lutz Vossebein¶, Grazia Tamma‖, Michael Beyermann‡, Eberhard Krause‡, Friedrich W. Herberg¶, Giovana Valenti‖, Sebastian Bachmann§, Walter Rosenthal‡, and Enno Klussmann‡**‡‡**

*From the ‡Forschungsinstitut für Molekulare Pharmakologie, Campus Berlin-Buch, Robert-Rössle-Strasse 10, 13125 Berlin, Germany, the §Institut für Anatomie, Charité, Universitätsmedizin Berlin, Campus Mitte, Humboldt-Universität zu Berlin, Philippstrasse 12, 10117 Berlin, Germany, the ¶Abteilung Biochemie, Universität Kassel, Heinrich-Plett-Strasse 40, 34132 Kassel, Germany, the ‖Dipartimento di Fisiologia Generale e Ambientale, Universita de Bari, Via Amendola 165/A, 70126 Bari, Italy, and the **Institut für Pharmakologie, Charité, Universitätsmedizin Berlin, Campus Benjamin Franklin, Freie Universität Berlin, Thielallee 67-73, 14195 Berlin, Germany*

Arginine vasopressin (AVP) increases the water permeability of renal collecting duct principal cells by inducing the fusion of vesicles containing the water channel aquaporin-2 (AQP2) with the plasma membrane (AQP2 shuttle). This event is initiated by activation of vasopressin V2 receptors, followed by an elevation of cAMP and the activation of protein kinase A (PKA). The tethering of PKA to subcellular compartments by protein kinase A anchoring proteins (AKAPs) is a prerequisite for the AQP2 shuttle. During the search for AKAP(s) involved in the shuttle, a new splice variant of AKAP18, AKAP18δ, was identified. AKAP18δ functions as an AKAP *in vitro* and *in vivo*. In the kidney, it is mainly expressed in principal cells of the inner medullary collecting duct, closely resembling the distribution of AQP2. It is present in both the soluble and particulate fractions derived from renal inner medullary tissue. Within the particulate fraction, AKAP18δ was identified on the same intracellular vesicles as AQP2 and PKA. AVP not only recruited AQP2, but also AKAP18δ to the plasma membrane. The elevation of cAMP caused the dissociation of AKAP18δ and PKA. The data suggest that AKAP18δ is involved in the AQP2 shuttle.

Many hormones influence cellular functions by elevating intracellular cAMP, thereby activating protein kinase A (PKA).[1] The inactive PKA holoenzyme is a tetramer consisting of a dimer of regulatory subunits each of which binds a catalytic subunit. Binding of cAMP to the regulatory subunits results in dissociation of the catalytic subunits that then phosphorylate their substrates (1–3). As PKA and many of its substrates are present throughout the cell, it is unclear how a raise of cAMP and the subsequent activation of PKA elicits a timely and spatially orchestrated cellular response. One mechanism is the compartmentalization of PKA, mediated by protein kinase A anchoring proteins (AKAPs), a family of distinct but functionally conserved proteins. AKAP-mediated tethering of PKA to subcellular compartments is thought to localize PKA to specific sites and limit its access to a subset of substrates (4–6). The activation of AKAP-anchored PKA by cAMP in discrete microdomains has recently been visualized in neonatal cardiomyocytes (7).

AKAP18 comprises a family of splice variants including AKAP18α, -β, and -γ (Fig. 1). AKAP18α (8), also known as AKAP15 (9, 10), consists of 81 amino acid residues. It anchors PKA to the basolateral plasma membrane of epithelial cells through a canonical RII-binding domain and interacts with L-type Ca^{2+} channels in skeletal muscle cells and cardiomyocytes through a leucine zipper motif, thereby facilitating L-type Ca^{2+} channel phosphorylation by PKA (9–14). The phosphorylation increases the open probability of the channel. AKAP18α may also potentiate insulin secretion from pancreatic β-cells (8). In addition, AKAP18α interacts with brain Na^+ channels, thereby enabling channel phosphorylation and down-regulation by PKA (15, 16). AKAP18β consists of 104 amino acid residues. Its cellular function is unclear. AKAP18α and AKAP18β share an identical membrane targeting domain, consisting of the N-terminal residues Gly-1, Cys-4, and Cys-5, modified by myristoylation and dual palmitoylation, respectively (8, 17). Compared with AKAP18α, AKAP18β possesses an additional 23-amino acid domain, directing it to the apical plasma membrane in polarized epithelial cells (17). AKAP18γ consists of 326 amino acid residues. Its distribution has so far been investigated in mouse oocytes and cellular fractions derived from rat kidney. In the kidney it is not only present in the particulate but also in the soluble fraction, in contrast to most AKAPs. AKAP18γ is assumed to associate in a regulated manner via an interacting protein with subcellular compartments (17). In mouse oocytes, AKAP18γ targets regulatory type I (RI)

* This work was supported by Deutsche Forschungsgemeinschaft Grants Ro597/6, Ro597/9, and He1818/3, the Fonds der Chemischen Industrie, and European Union Grants QLK3-CT-2002-02149 and QLRT-2000-00987. The costs of publication of this article were defrayed in part by the payment of page charges. This article must therefore be hereby marked "*advertisement*" in accordance with 18 U.S.C. Section 1734 solely to indicate this fact.

‡‡ To whom correspondence should be addressed: Forschungsinstitut für Molekulare Pharmakologie, Campus Berlin-Buch, Robert-Rössle-Str. 10, D-13125 Berlin, Germany. Tel.: 49-30-94793-260; Fax: 49-30-94793-109; E-mail: klussmann@fmp-berlin.de.

[1] The abbreviations used are: PKA, protein kinase A; AKAP, A-kinase anchoring protein; AQP2, aquaporin-2; AVP, arginine vasopressin; dDAVP, desmopressin; GST, glutathione *S*-transferase; IMCD, inner medullary collecting duct; PBS, phosphate-buffered saline; RII, regulatory type II; RACE, rapid amplification of cDNA ends; FRET, fluorescence resonance energy transfer; CFP, cyan fluorescent protein; GFP, green fluorescent protein; YFP, yellow fluorescent protein; MOPS, 4-morpholinepropanesulfonic acid.

PKA subunits to the nucleus, suggesting an involvement in transcriptional regulation (18).

Arginine vasopressin (AVP) is one of the numerous hormones acting through a receptor coupled to the G_s/adenylyl cyclase system. Binding of AVP to its cognate V2 receptor, located in the basolateral plasma membrane of renal collecting duct principal cells, results in the redistribution of the water channel aquaporin-2 (AQP2) from intracellular vesicles to the plasma membrane (AQP2 shuttle; for review see Refs. 19–21). This process constitutes the molecular basis of AVP-stimulated water reabsorption. Inactivating mutations in the *V2 receptor* or *AQP2* gene cause nephrogenic diabetes insipidus, a disease characterized by a massive loss of water (for review see Ref. 22). On the molecular level, AVP stimulates the elevation of cAMP followed by activation of PKA. PKA phosphorylates AQP2 at serine 256 (Ser-256). A mutation of this site (S256A) or inhibition of PKA prevents the AQP2 shuttle, indicating that the phosphorylation of AQP2 by PKA is an essential step (23–27). Three or more monomers in an AQP2 tetramer need to be phosphorylated at Ser-256 for the translocation to the plasma membrane to occur (28). Ser-256 is also a substrate for Golgi casein kinase and its phosphorylation by this kinase is required for Golgi transition (29). Phosphorylation of Ser-256 does not seem to have a functional consequence because the water permeability of AQP2 hardly changes upon phosphorylation (30, 31).

Besides phosphorylation of Ser-256, other maneuvers lead to a translocation of AQP2 to the plasma membrane. Inhibition of the small GTPases of the Rho family by bacterial toxins or disruption of F-actin with cytochalasin D in the absence of cAMP-elevating agents resulted in the accumulation of AQP2 at the plasma membrane of primary cultured rat inner medullary collecting duct (IMCD) cells and CD8 cells (32, 33), a rabbit cortical collecting duct cell line stably expressing rat AQP2 (34). The AVP- or forskolin-induced elevation of cAMP in IMCD and CD cells, however, also caused inhibition of RhoA and this is a prerequisite for the AQP2 shuttle (32, 33, 35). The underlying mechanism is PKA-mediated phosphorylation of RhoA (36). Another mechanism leading to accumulation of AQP2 in the plasma membrane in a phosphorylation-independent manner is inhibition of endocytosis by the GTPase-deficient dynamin mutant K44A or the cholesterol-depleting agent methyl-β-cyclodextrin. Both agents led to an accumulation of the phosphorylation-deficient AQP2 mutant S256A at the plasma membrane IMCD cells (37).

The finding by Lande *et al.* (31) that AQP2-bearing vesicles contain PKA activity led us to investigate whether anchoring of PKA to AKAPs is required for the AQP2 shuttle. Using primary cultured rat IMCD cells as a model system (38) and the membrane-permeable anchoring inhibitor peptide S-Ht31, we have shown that the anchoring of PKA to AKAPs is a prerequisite for the AQP2 shuttle (26, 39). We report here the identification and characterization of a new splice variant of AKAP18, AKAP18δ, and provide evidence for its involvement in the AQP2 shuttle.

EXPERIMENTAL PROCEDURES

Screening of an Expression cDNA Library, PCR, RACE-PCR, and DNA Sequence Analysis—A rat kidney Uni-ZAP XR expression cDNA library (Stratagene, La Jolla, CA) was screened, using the RII overlay technique (40). A partial cDNA clone (clone 9.1) was isolated. To obtain the upstream coding sequence, 5′-RACE PCR was carried out using rat heart Marathon-Ready cDNA as template and the Advantage cDNA polymerase mixture (BD Biosciences, Heidelberg, Germany). The forward primers were supplied with Marathon-Ready cDNA; the reverse primer annealed with bp 438–414 or 462–438 of AKAP18δ. RACE-PCR products were cloned into the vector pGEM-T Easy (Promega, Madison, WI) and sequenced by primer walking starting with vector sequencing primers. Homology searches were performed via the World Wide Web at GenBank™, National Center for Biotechnology Information, sequence translations and alignments at the Human Genome Center, Baylor College of Medicine (BCM Search Launcher).

Generation of Glutathione S-Transferase Fusion Proteins—For generating a plasmid encoding a fusion protein consisting of the full-length AKAP18δ and gluthatione *S*-transferase (GST), the coding region of AKAP18δ was amplified from rat heart Marathon-Ready cDNA (BD Biosciences) by PCR. A fragment encoding AKAP18δ amino acid residues 124–353 was generated by PCR using the full-length AKAP18δ as template. All forward and reverse primers contained EcoRI and XhoI restriction sites, respectively. The cDNAs were cloned into the vector pGEX-4T-3 (Amersham Biosciences, Freiburg, Germany) to yield GST-AKAP18δ and GST-AKAP18δ-(124–353). GST fusion proteins were expressed in *Escherichia coli* (strain BL21), affinity purified as recommended by the supplier of the pGEX-4T-3 vector (Amersham Biosciences), and used for Western blotting (see below) and RII overlay assays (see below).

Surface Plasmon Resonance Measurements—Surface plasmon resonance measurements were carried out as described (41), using a Biacore 2000 instrument (Biacore Intl. AB, Uppsala, Sweden). In brief, CM-5 chips (research grade, Biacore AB), coated with 8-aminohexylamino-cAMP (Biolog, Bremen, Germany), were used to capture cAMP-free human regulatory PKA RIα, RIβ, RIIα, or RIIβ subunits (surface concentration of 120–200 resonance units for each subunit). All subsequent interaction studies were performed in running buffer (20 mM MOPS, 150 mM NaCl, pH 7.0, containing 0.005% surfactant P20) at 20 °C. Unspecific binding was subtracted using blank runs performed on an NHS/EDC-activated and ethanolamine-deactivated surface, and a surface immobilized with 8-aminohexylamino-cAMP with no R-subunit was captured. The fusion proteins GST-AKAP18δ and GST-AKAP18δ-(124–353) (see above) were injected into the flow chamber of the Biacore instrument (flow of 30 μl/min) in a series of dilutions (12 nM to 1 μM; for 300 s) to determine association and dissociation rates. After injection, the dissociation phase in the absence of AKAPs was monitored for 600 s. After subtraction of signals obtained from blank runs, kinetic constants from the raw data were calculated by non-linear regression or equilibrium binding analysis using Biaevaluation software version 3.1 (Biacore). Equilibrium binding constants (K_D) were calculated from the respective rate constants on the basis of a Langmuir 1:1 binding model. The nonlinear regressions were fitted using global fit analysis.

Fluorescence Resonance Energy Transfer (FRET) Measurements—For generating a plasmid encoding a fusion protein of AKAP18δ with the cyan fluorescent protein (CFP), AKAP18δ-CFP, full-length AKAP18δ was amplified by PCR using GST-AKAP18δ (see above) as template and forward and reverse primers containing EcoRI and BamHI restriction sites, respectively, and subcloned into the vector pECFP-N1 (BD Biosciences). The cDNA encoding human PKA regulatory subunit type IIα (RIIα) was a generous gift of Dr. K. Tasken (University of Oslo, Norway). For generating plasmids encoding a fusion protein of RIIα and the yellow fluorescent protein (YFP), RIIα-YFP, full-length RIIα was amplified using a forward primer with a restriction site for XhoI and a reverse primer with a restriction site for BamHI. The cDNA was subcloned into the vector pEYFP-N1 (BD Biosciences). To substitute a leucine for a proline residue (AKAP18δ-L308P) in the RII-binding domain of AKAP18δ-CFP, site-directed mutagenesis was performed using the QuikChange Site-directed Mutagenesis Kit (Stratagene, La Jolla, CA). All constructs were sequenced prior to expression.

HEK293 cells (ATCC, Manassas, VA) were grown to 40–60% confluency on poly-L-lysine-coated 30-mm coverslips in Dulbecco's modified Eagle's medium supplemented with 10% fetal calf serum. CD8 cells were grown as described (29, 34, 35). HEK293 and CD8 cells were transiently co-transfected with the plasmids encoding RIIα-YFP and either AKAP18δ-CFP or AKAP18δ-L308P-CFP (1–2 μg of plasmid DNA) using LipofectAMINE (Invitrogen, Groningen, The Netherlands).

In HEK293 cells FRET was measured with an epifluorescence microscope (Axiovert 200M, Carl Zeiss, Göttingen, Germany) equipped with a digital camera (Hamamatsu Photonics, Herrsching am Ammersee, Germany) using a monochromator Polychrome IV (TILL-Photonics, Martinsried, Germany). Data were recorded with the Openlab 2.25 Software (Improvision, Coventry, England). In CD8 cells FRET was measured with an epifluorescence microscope (TE 2000S, Nikon Instruments, Florence, Italy) equipped with a CCD camera (MicroMax 512BFT, Princeton Instruments, Princeton, NJ) using a DeltaRAM Highspeed Multiwavelength Illuminator for excitation (Photon Technology International, Lawrenceville, NJ). Data were recorded and processed with the MetaMorph/MetaFluor software (Universal Imaging

Corp., Downington, PA). CFP and YFP were excited at 425 or 488 nm, respectively; fluorescence emitted from CFP and YFP was measured at 480/30 and 535/26 nm, respectively. FRET from CFP to YFP was determined by excitation of CFP (425 nm) and measurement of fluorescence emitted from YFP (535/26 nm). The maximum FRET capability of the system was defined by determining FRET from CFP to YFP in a fusion protein consisting of the two proteins (42). Background fluorescence from a region with no cells was subtracted from the data. A ratio of 535/480 nm >0.6 was considered a positive FRET signal. As a negative control CFP and YFP were expressed as soluble proteins by co-transfection of vectors pECFP-N1 and pEYFP-N1. The specificity of FRET signals from RIIα-YFP to AKAP18δ-CFP was tested by measuring FRET in the presence of the membrane-permeable anchoring inhibitor peptide S-Ht31 (100 μM; see "Introduction") or the inactive peptide S-Ht31-P (control). In addition, FRET signals were verified by measurement of donor recovery after acceptor bleaching. For this purpose, YFP was bleached by pulses of light at 488 nm, and the CFP emission at 480/30 nm was measured simultaneously.

RNA Isolation and Northern Blotting—A multiple tissue Northern blot was sequentially hybridized with a PCR-generated, [α-^{32}P]dCTP-labeled cDNA fragment of AKAP18δ (bp 20 to 164), and [α-^{32}P]dCTP-labeled β-actin according to the supplier's recommendations (BD Biosciences).

Total RNA from rat renal inner medulla and residual kidney tissue was isolated using peqGold RNApure (peqLab Biotechnologie, Erlangen, Germany). Northern blotting was carried out using a sodium phosphate-buffered gel system (43). The blot was sequentially hybridized with a [α-^{32}P]dCTP-labeled EcoRI/HindIII fragment of the AKAP18δ cDNA (bp 320–1723) and [α-^{32}P]dCTP-labeled β-actin. Labeling reactions were performed using the Megaprime labeling kit (Amersham Biosciences). Radioactive signals were detected by autoradiography (Kodak X-OMAT x-ray films).

Preparation of Affinity Purified Anti-AKAP18δ and Anti-AQP2 Antibodies—A rabbit polyclonal antiserum (A18δ4) was raised against a peptide corresponding to amino acid residues 1–33 of AKAP18δ (Biogenes, Berlin, Germany). An anti-AQP2 antiserum (2051) was raised as described (44). Specific antibodies were isolated by affinity chromatography of the antisera over the peptides used for immunization (coupled to thiopropyl-Sepharose 6B; Amersham Biosciences).

Preparation of Subcellular Fractions, Immunoprecipitation, and cAMP-agarose Pull-down—Rat kidney inner medullae were homogenized in lysis buffer (10 mM K_2HPO_4, 150 mM NaCl, 5 mM EDTA, 5 mM EGTA, 1% Triton X-100, 0.2% deoxycholate, 1 mM benzamidine, 0.5 mM phenylmethanesulfonyl fluoride, 3.2 μg/ml trypsin inhibitor I-S, 1.4 μg/ml aprotinin). The lysates were cleared by centrifugation (30,000 × *g*, 4 °C, 30 min). For immunoprecipitations affinity-purified antibody A18δ4 or the corresponding preimmune serum and protein A-conjugated agarose (Sigma Deisenhofen, Germany) were added. For cAMP-agarose pull-down experiments the lysates were incubated with cAMP-agarose (4 °C, 3 h; Biolog, Bremen, Germany) in the absence or presence of cAMP (50 mM; Ref. 45). Proteins bound to protein A- or cAMP-conjugated agarose were washed four times with lysis buffer and eluted with Laemmli sample buffer (95 °C). To obtain particulate and soluble fractions, renal inner medullae, homogenized in phosphate-buffered saline (PBS) and cleared from cell debris and nuclei (4,000 × *g*, 4 °C, 10 min), were centrifuged (150,000 × *g*, 4 °C, 1 h). The supernatant and the pellet, resuspended in lysis buffer, were considered soluble and particulate fractions, respectively. Proteins were analyzed by Western blotting and RII overlay assay (see below).

Immunoisolation of Intracellular Vesicles—Affinity-purified A18δ4 antibody was coupled to Eupergit C1Z methacrylate microbeads (Roehm Pharma, Darmstadt, Germany) according to the procedure described (46), yielding AKAP18AB beads. Non-saturated binding sites were blocked by incubation with glycine. As a control, beads were coated with glycine alone (glycine beads). Rat renal inner medullae were homogenized in homogenization buffer (250 mM sucrose, 3 mM imidazol, pH 7.5). Nuclei and cell debris were removed by centrifugation (3,000 × *g*, 4 °C, 15 min), and the resulting postnuclear supernatants were incubated with AKAP18AB or glycine beads while rotating (45 min, 4 °C). The beads were recovered by centrifugation (3,000 × *g*, 4 °C, 5 min) through a sucrose cushion (0.8 M). The supernatants were discarded and the pellets were washed by 5 rounds of resuspending in PBS and subsequent centrifugation (3,000 × *g*, 4 °C, 5 min). The final pellets were resuspended in Laemmli sample buffer and subjected to Western blotting (see below).

Western Blotting and RII Overlay—Western blotting was carried out as described (35). In brief, AKAP18δ was detected with the affinity-purified antibody A18δ4 and horseradish peroxidase-conjugated goat anti-rabbit F(ab)$_2$ fragments as secondary antibody (Dianova, Hamburg, Germany). PKA RIIβ subunits were detected using commercially available monoclonal antibodies (BD Biosciences) and secondary horseradish peroxidase-conjugated goat anti-mouse antibodies (Chemicon International, Hofheim, Germany). AQP2 was detected using rabbit antiserum 2051 and horseradish peroxidase-conjugated goat anti-rabbit F(ab)$_2$ fragments as secondary antibody (26, 44). The commercially available antibodies directed against AQP4 (Biotrend Chemikalien, Cologne, Germany), calreticulin (Dianova), and α-tubulin (Oncogene Research Product, Calbiochem, Cambridge, MA) were applied according to the manufacturer's instructions and detected with the secondary horseradish peroxidase-conjugated antibodies given above. Signals were visualized with the Lumi-Imager F1 (Roche Diagnostics, Mannheim, Germany). RII overlays were carried out using radioactively labeled RII subunits (26, 40).

Detection of AQP2 and AKAP18δ in Primary Cultured IMCD Cells—Primary cultured rat IMCD cells were obtained from rat renal inner medullae and cultured as described (38, 47). The culture medium was routinely supplemented with 500 μM dibutyryl cAMP for the maintenance of AQP2 expression. Dibutyryl cAMP was removed 16 h prior to experiments, which were performed 6 days after seeding.

AQP2 was detected using polyclonal goat anti-AQP2 antibody (Santa Cruz, Heidelberg, Germany) and Cy5-conjugated donkey anti-goat antibody (Dianova). AKAP18δ was detected with affinity-purified rabbit antibody A18δ4 (1:50) and Cy3-conjugated mouse anti-rabbit antibody (Dianova). As a control, antibody A18δ4 was preincubated with a 1,000-fold molar excess of the peptide used for the immunization. Signals were visualized by confocal laser scanning microscopy (LSM 510; Carl Zeiss). For quantification of the effects of AVP on the localization of AQP2 and AKAP18δ, the ratio of intracellular/plasma membrane fluorescence signal intensities was calculated as described (26, 32, 35). For all groups, mean ± S.E. values were calculated. Statistical analyses were performed using the Student's *t* test and one-way analysis of variance (26, 32, 35).

For immunogold electron microscopy IMCD cells were grown on Transwell filters, fixed (0.25% glutaraldehyde, 3% formaldehyde), cryosubstituted in a Leica AFS freeze-substitution unit, and embedded in LR-White. Briefly, the samples were sequentially equilibrated over 4 days in methanol at temperatures gradually increasing from −90 to −45 °C. The samples were infiltrated with LR-White for 72 h at −20 °C, and polymerized for 1 h at −20 °C and 2 h at 4 °C. Sections (60 nm) were cut on a Reichert Ultracut S, placed on nickel grids, and blocked with glycine. The sections were incubated with goat anti-AQP2 antibody (1:10; Santa Cruz) and affinity-purified rabbit anti-AKAP18δ A18δ4 antibody (1:25) for 1 h at room temperature. The sections were washed with PBS and incubated with donkey anti-goat antibody (1:20; Dianova) and donkey anti-rabbit antibody (1:10; Dianova) coupled to 12- and 18-nm gold grains, respectively (Dianova). Thereafter, sections were stained with uranyl acetate and lead citrate. The sections were analyzed with a 80-kV electron microscope (902A, LEO, Obercochem, Germany) equipped with a slow scan CCD camera (Megaview III, Soft Imaging System, Germany) and the analySIS software (Soft Imaging System). The percentages of vesicles containing AQP2, AKAP18δ, or both were determined by analyses of images from two independent experiments. Unlabeled vesicles were disregarded. For quantification of the effects of AVP on the localization of AQP2 and AKAP18δ, gold particles/μm of plasma membrane were determined in images obtained from two independent experiments. For all groups the means were calculated.

Detection of AQP2 and AKAP18δ in Kidney Sections—Sprague-Dawley rats were supplied with drinking water containing 180 mM sucrose for 48 h to achieve a good hydration status. Desmopressin (dDAVP; 1 μg/ml saline) or saline alone (control) were administered subcutaneously. After 2 h, the rats were sacrificed by *in vivo* perfusion fixation under phenobarbital anesthesia. The kidneys were removed, cut into slices, shock frozen, and embedded.

Cryo-sections (2–4 μm) were prepared and blocked with PBS containing 5% skim milk, pH 7.4. Sections were incubated with affinity-purified antibody A18δ4 (2 h at room temperature and then overnight at 4 °C), followed by incubation with fluorescein isothiocyanate-conjugated mouse anti-rabbit antibody (Dianova). As a control, antibody A18δ4 was preincubated with a 1,000-fold molar excess of the peptide used for the immunization. The sections were washed with PBS and sequentially incubated with goat anti-AQP2 antibody (1:200, 2 h, room temperature; Santa Cruz) and Cy3-conjugated donkey anti-goat antibody (Dianova). Nuclei were stained with 4′,6-diamino-2-phenylindole (Sigma) diluted in PBS. After washing with PBS, sections were analyzed using a Leica DMLB epifluorescence micro-

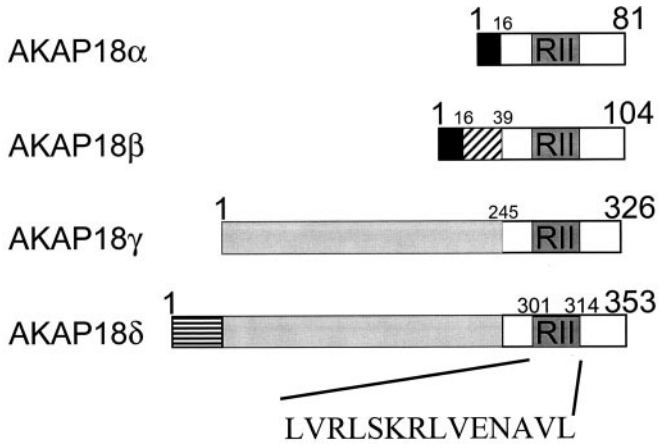

FIG. 1. **Schematic representation of AKAP18 isoforms.** Amino acid residues (one-letter code) are indicated by *numbers*. The membrane targeting domains of AKAP18α and -β (*black*) and the RII-binding sites (RII) of all isoforms are identical. Amino acids 1–245 of AKAP18γ and 27–272 of AKAP18δ are homologous (*gray*). The N terminus of AKAP18δ (amino acids 1–26, *horizontal stripes*) is unique to this isoform.

scope equipped with a CCD camera (Leica Microsystems, Wetzlar, Germany).

RESULTS

Molecular Cloning of AKAP18δ, a New Splice Variant of AKAP18—To identify AKAPs involved in the AQP2 shuttle, a rat kidney cDNA expression library was screened using the RII overlay technique. One of the cDNAs isolated was 2655 bp long and encoded an open reading frame of 262 amino acids. The lack of a start codon indicated an incomplete cDNA. 5′-RACE PCR with Marathon cDNA from rat heart as template yielded a full-length cDNA (2975 bp). The start codon is located within a Kozak consensus sequence (gcgaccATGg; Ref. 48), and the stop codon (bp 1116–1118) is followed by a polyadenylation signal (bp 2938–2945, aataaa) and a poly(A) tail (stretch of 17 adenosines), starting 15 bp downstream of the polyadenylation signal. The complete cDNA encodes a protein of 353 amino acids (Fig. 1; GenBank™ accession number AY350741). Blast homology searches (GenBank™, NCBI) revealed amino acid sequence identities in the overlapping regions of 76.6% with human AKAP18α, 76.6% with AKAP18β, 75% with AKAP18γ (17), and 100% with mouse AKAP18α (8). The data indicate that the isolated cDNA represents a new splice variant of AKAP18, which we named AKAP18δ (Fig. 1; GenBank™ accession number AY350741).

Recombinant AKAP18δ Functions as an AKAP—AKAP18δ contains an amino acid sequence (residues 301 to 314; Fig. 1) identical with the amino acid sequence of the RII-binding domains of AKAP18α, -β, and -γ (8, 17). Using truncated versions of AKAP18δ in RII overlay assays, the RII-binding domain of AKAP18δ was mapped to a region between amino acids 299 and 353. Thus, it is most likely identical with the RII-binding domain of AKAP18α, -β, and -γ (data not shown).

The kinetics (association and dissociation rates) for the binding of full-length AKAP18δ fused to GST and GST-AKAP18δ-(124–353) to RIIα and RIIβ subunits were determined by surface plasmon resonance measurements (Fig. 2; Ref. 41). The K_D values determined for the binding of RIIα and RIIβ subunits to full-length AKAP18δ were 31 and 20 nM, respectively (Table I). Several AKAPs, including AKAP-Lbc/Ht31, AKAP79, and AKAP95, bind RII subunits with K_D values of 1.3–50 nM (41, 49, 50) and are considered as high affinity AKAPs. In contrast, AKAPs such as gravin or the members of the ezrin radixin moesin family bind RII subunits with lower affinity (μM range) and are considered low affinity AKAPs (51). Thus, AKAP18δ is a high affinity AKAP. The K_D for the binding of GST-AKAP18δ-(124–353) to the RII subunits (9 and 4 nM for RIIα and RIIβ, respectively) is 4–5 times lower than that of full-length AKAP18δ. This may result from steric hindrance by the N-terminal portion of the full-length protein, limiting access of RII subunits to the C-terminal RII-binding site (41).

Endogenous AKAP18δ Functions as an AKAP—Fig. 3*A* shows an RII overlay assay. Antibody A18δ4 (see "Experimental Procedures") immunoprecipitated a prominent 50-kDa RII-binding protein from rat renal inner medulla homogenates (Fig. 3*A*, *left panel*). The protein was not detectable if the RII overlay assay was carried out in the presence of the anchoring inhibitor peptide Ht31 (*right panel*) and, thus, most likely represents the endogenous AKAP18δ. The immunoprecipitate contained an additional RII-binding protein of about 55 kDa corresponding in size to RII subunits that are expected to co-immunoprecipitate with AKAP18δ. Membrane-bound RII subunits are detectable because of dimerization with the radioactively labeled RII subunits of the probe (52). The proteins were not precipitated by the preimmune serum.

To further test the AKAP function of AKAP18δ, cAMP-agarose pull-down experiments with rat renal inner medulla homogenates were carried out (Fig. 3, *B* and *C*). Cyclic AMP-agarose efficiently pulled down RIIβ subunits (Fig. 3*B*, *lane 1*) and a protein recognized by antibody A18δ4 (Fig. 3*C*, *lane 1*). The precipitated protein corresponded in size to recombinant AKAP18δ (*lane 3*), suggesting that it represents the endogenous AKAP18δ. If antibody A18δ4 was preincubated with the peptide used for immunization, the precipitated AKAP18δ was not detected and the recombinant AKAP18δ only weakly (*lanes 4* and *6*). As a further control, cAMP-agarose pull-down experiments were carried out in the presence of cAMP. Under this condition, neither RII subunits (Fig. 3*B*, *lane 2*) nor AKAP18δ were detectable (Fig. 3*C*, *lanes 2* and *5*).

AKAP18δ Is Present in the Soluble and Particulate Fractions Prepared from Rat Renal Inner Medullae—Cyclic AMP-agarose efficiently pulled down RIIβ subunits from soluble and particulate (150,000 × *g* pellet) fractions of rat renal inner medulla (Fig. 4, *upper panel*). AKAP18δ was abundantly present in the precipitates from the soluble fraction and was merely detectable in the particulate fraction (Fig. 4, *lower panel*). The preimmune serum did not recognize a protein in the precipitate (data not shown).

Interaction of AKAP18δ and RIIα Subunits in Living Cells (FRET Technique)—A fusion protein consisting of CFP and YFP was expressed in HEK293 cells and FRET from CFP to YFP was determined to define the maximum FRET signal obtainable in this system (Fig. 5*A*, *upper left panel*). The FRET signal is depicted as the ratio of 535/480 nm in false colors (ratio = 1.2–1.5, Fig. 5*A*). Co-expression of soluble CFP and YFP did not yield a positive FRET signal (ratio < 0.6, Fig. 5*A*, *middle left panel*), indicating that CFP and YFP need to be in close proximity (<10 nm) and physically associated for FRET to occur.

Subsequently, the FRET technique was applied to visualize the interaction of AKAP18δ with regulatory RII subunits in HEK293 cells (Fig. 5, *B–E*). The cells were co-transfected with plasmids encoding RIIα-YFP and AKAP18δ-CFP. Fig. 5*B* shows a mainly cytosolic distribution of RIIα and AKAP18δ fusions (*upper left* and *right panels*, respectively). The *lower left panel* shows the FRET signal (fluorescence emitted by YFP in the same cells shown in the *upper panel* after excitation of CFP at 425 nm). The FRET ratio (ratio 535/480 nm = 1.2–1.5) is depicted in false colors (*lower right panel*). The membrane-permeable (stearated) anchoring inhibitor peptide S-Ht31 (100

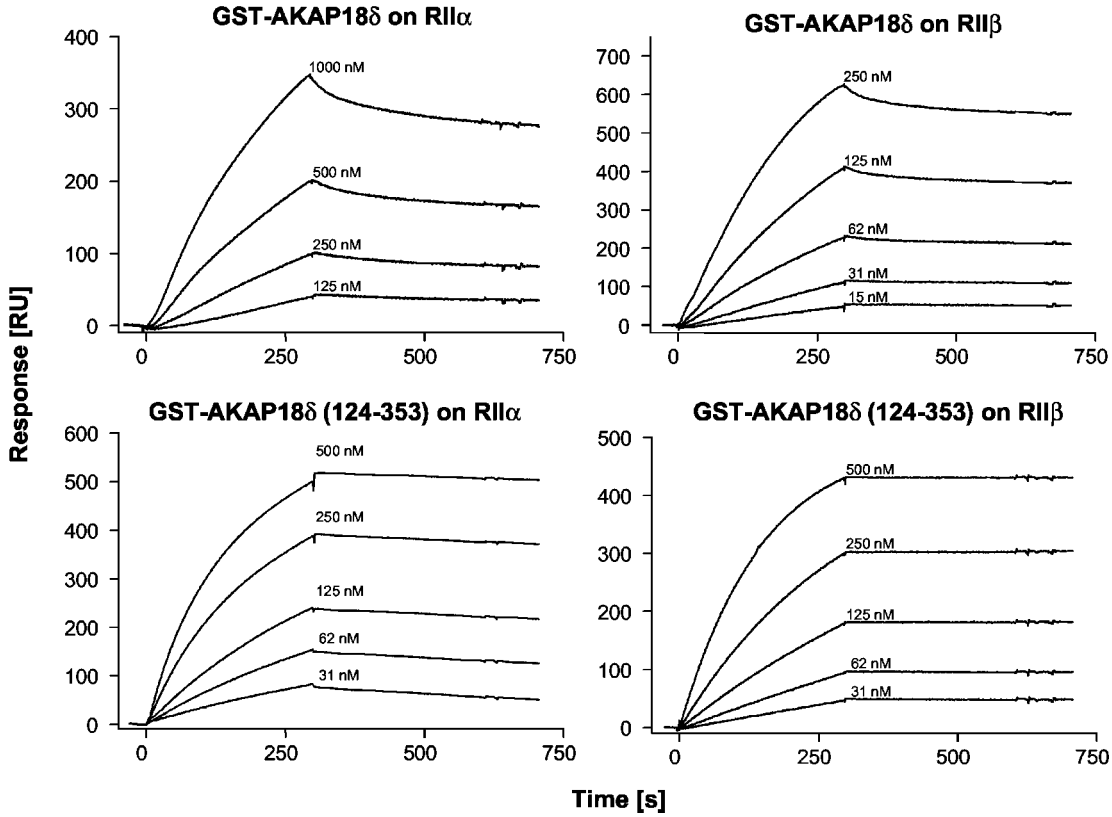

FIG. 2. **AKAP18δ functions as an AKAP *in vitro*.** Surface plasmon resonance measurements to determine the association and dissociation rate constants (see Table I) for the binding of GST-AKAP18δ and GST-AKAP18δ-(124–353) to human PKA regulatory RII subunits. The plots show representative experiments for each interaction. Each experiment was repeated at least three times using different protein preparations and different immobilization rates of the regulatory subunits.

TABLE I

Apparent rate and equilibrium binding constants of the interaction of human RIIα and RIIβ subunits with full-length AKAP18δ and amino acids 124–353 of AKAP18δ

The AKAP proteins were fused to GST. Apparent association (k_a) and dissociation (k_d) rate constants were calculated from at least three independent experiments using global fit analysis as described under "Experimental Procedures."

	k_a	k_d	K_D
	$mol^{-1} \times s^{-1}$	s^{-1}	nM
AKAP18δ			
RIIα	2×10^4	6.7×10^{-4}	31
RIIβ	1.8×10^4	3.5×10^{-4}	20
AKAP18δ-(124–353)			
RIIα	2.6×10^4	2.3×10^{-4}	9
RIIβ	1.2×10^4	4×10^{-5}	4

μm; Ref. 26) significantly decreased the FRET signal in a time-dependent manner (ratio = 0.55 ± 0.14; mean ± S.E.; seven independent experiments; Fig. 5, *C* and *E*). The inactive (proline-containing) peptide S-Ht31-P (100 μm; Ref. 26) did not influence the FRET signal (ratio = 1.32 ± 0.16; eight independent experiments; Fig. 5, *D* and *E*).

The peptide S-Ht31 did not change the FRET signal in HEK293 cells expressing the CFP-YFP fusion protein, neither did it induce a FRET signal from soluble CFP to soluble YFP or from AKAP18δ-CFP to soluble YFP (Fig. 5*A*). The specificity of the FRET signal was also verified by measuring donor recovery after acceptor bleaching (CFP fluorescence increased by 9.9% after bleaching of YFP, data not shown). Thus, the FRET signal stems from the interaction of AKAP18δ with RIIα subunits.

The substitution of leucine 308 in the putative RII-binding domain of AKAP18δ by proline reduced the FRET signal compared with the one obtained with wild-type AKAP18δ-CFP (ratio = 0.79 ± 0.07; three independent experiments). The data confirm that the RII-binding domain of AKAP18δ is identical with that of the other AKAP18 variants.

Tissue Expression Pattern of AKAP18δ—The AKAP18δ expression pattern was investigated by multiple rat tissue Northern blot analysis utilizing bp 20–164 of the AKAP18δ cDNA as a probe (Fig. 6*A*, *upper panel*). Three major transcripts of ~2.3, 3, and 3.5 kb were detected in most tissues. The length of the 3-kb transcript is similar to that of the AKAP18δ cDNA (2975 bp), and thus most likely represents the corresponding mRNA. The 2.3- and 3.5-kb mRNAs may represent additional AKAP18 isoforms. The expression levels of the 3-kb putative AKAP18δ transcript was highest in the heart. In brain, lung, liver, kidney, and testis it was expressed at comparable levels. In spleen and skeletal muscle the transcript was hardly detectable. The 2.3-kb transcript was expressed in heart at a similar level as the 3-kb transcript. It was, as the 3.5-kb transcript, weakly expressed in spleen and skeletal muscle. Similar to the putative AKAP18δ mRNA, the 2.3- and 3.5-kb mRNAs were expressed at comparable levels in brain, lung, liver, kidney, and testis. The minor differences in signal intensities observed are most likely because of unequal loading of mRNA, as is suggested by the β-actin control (Fig. 6*A*, *lower panel*).

As AVP mainly exerts its antidiuretic action in the renal inner medulla (main expression site of AQP2), we compared levels of the 3-kb putative AKAP18δ mRNA in rat renal inner medulla and residual kidney tissue. A cDNA probe (bp 320–1732 of AKAP18δ), potentially hybridizing to AKAP18α, -β, -γ, and -δ, detected a 3- and ~2.3-kb transcript in the inner medulla (Fig. 6*B*, *upper panel*). Both mRNAs were weakly detectable in residual kidney tissue. The 3.5-kb transcript detected in the poly(A)$^+$ RNA preparation from kidney (see Fig. 6*A*) was

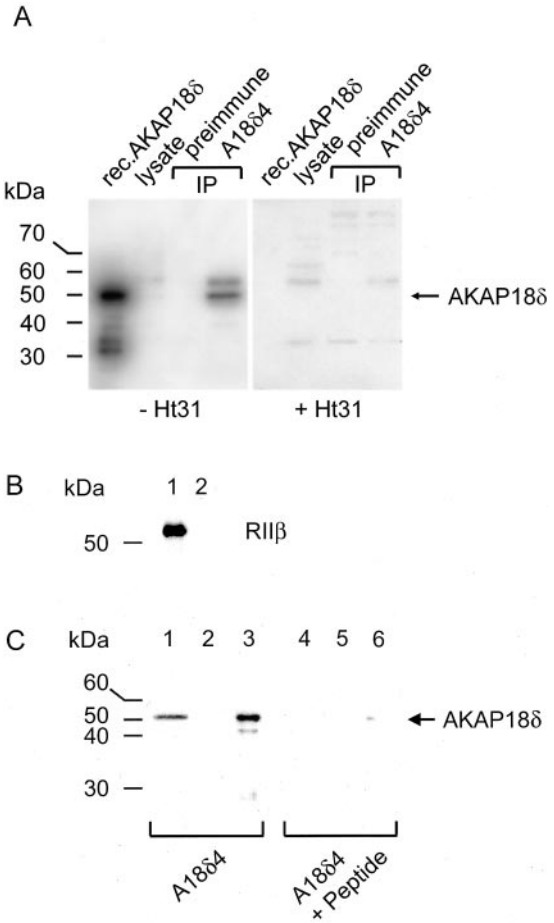

FIG. 3. **AKAP18δ functions as an AKAP *in vivo*.** *A*, lysates from rat renal inner medulla were prepared and subjected to immunoprecipitation (*IP*) with antibody A18δ4 or preimmune serum. The lysates, precipitates, and recombinant (*rec.*) AKAP18δ were probed in RII overlay assays carried out in the absence or presence of the anchoring inhibitor peptide Ht31. *B*, cAMP-agarose precipitates were obtained from rat renal inner medulla lysates in the absence (*lane 1*) or presence (*lane 2*) of cAMP. RIIβ subunits were detected by Western blotting. *C*, cAMP-agarose precipitates were isolated from rat renal inner medulla lysates in the absence (*lanes 1* and *4*) or presence of cAMP (*lanes 2* and *5*). *Lanes 3* and *6*, recombinant AKAP18δ. Western blotting was carried out with the affinity-purified antibody A18δ4 and A18δ4 preincubated with the peptide used for immunization.

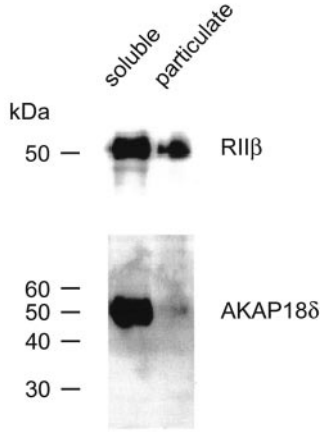

FIG. 4. **Detection of AKAP18δ in soluble and particulate compartments of renal inner medulla.** Soluble and particulate fractions derived from rat renal inner medulla were subjected to cAMP-agarose pull-down analysis. RIIβ subunits and AKAP18δ were detected by Western blotting with commercially available anti-RIIβ and affinity-purified A18δ4 antibodies, respectively.

not detected in the preparations of total RNA used for this experiment (Fig. 6*B*), most likely because the amount is too low.

AQP2, PKA Subunits, and AKAP18δ Reside on the Same Vesicles—The presence of AKAP18δ in the particulate fraction of renal inner medullary tissue (Fig. 4) and its abundant expression in renal inner medulla (Fig. 6) led us to investigate whether the AKAP is associated with AQP2-bearing vesicles. To this end we established a procedure to immunoisolate intracellular vesicles from rat renal inner medulla with antibody A18δ4 (AKAP18AB beads; see "Experimental Procedures"). Compared with the control (glycine beads), AQP2, regulatory RIIβ subunits of PKA (Fig. 7*A*, Western blot) and a prominent 50-kDa AKAP (Fig. 7*B*, RII overlay) were enriched in the vesicle fraction obtained with AKAP18AB beads. The size of the 50-kDa AKAP corresponds to that of recombinant AKAP18δ, suggesting that it represents AKAP18δ (*first lane*, Fig. 7*B*). The vesicular fraction did not contain detectable amounts of proteins from other cellular compartments. The water channel AQP4 (nonglycosylated form), a marker for the plasma membrane, tubulin, a cytoskeletal protein, or calreticulin, a marker for the endoplasmic reticulum were not detected in the fraction obtained with AKAP18AB. In a further series of experiments using a second anti-AKAP18δ antibody (A18δ3) similar observations were made (data not shown). The data provide strong evidence for the association of an AKAP18δ fraction with AQP2-bearing vesicles.

AQP2 and AKAP18δ Co-localize in IMCD Cells and Co-translocate to the Plasma Membrane in Response to AVP Stimulation—IMCD cells contain the molecular machinery for the AQP2 shuttle and respond to AVP by insertion of AQP2 into the basolateral plasma membrane (Fig. 8) (26, 32, 35, 47, 53, 54). Whereas in control cells, AQP2 was found mainly intracellularly, it was predominantly located at the plasma membrane in AVP-treated cells (Fig. 8*A*). Similarly, AKAP18δ was located intracellularly in control cells and associated with the plasma membrane in AVP-treated IMCD cells (Fig. 8*A*). After preincubation of antibody A18δ4, selectively recognizing AKAP18δ, with the peptide used for immunization, the signal was strongly reduced (Fig. 8*A*, *lower panels*). Consistent with the finding that AKAP18δ is mainly found in the cytosol (Fig. 4) and not exclusively on AQP2-bearing vesicles, the redistribution of AKAP18δ in response to AVP was less complete compared with that of AQP2. Quantitative analysis of the immunofluorescence signals confirmed these observations (Fig. 8*B*). The co-localization of AQP2 and AKAP18δ and their co-translocation in response to AVP were also confirmed by immunoelectron microscopy with sections from control and AVP-treated IMCD cells (Fig. 8*C*). Both the anti-AQP2 and anti-AKAP18δ antibodies yielded signals in the nucleus (Fig. 8*C*). The anti-AQP2 antibody most likely labeled histone H2A1 (55) and detection of AKAP18δ in the nucleus is likely because of the nuclear localization signal in the AKAP18δ sequence, which may direct it to the nucleus. If antibody A18δ4 was preincubated with the peptide used for immunization, the signal was reduced by >90% (data not shown).

Similar observations were made in experiments with kidney sections derived from control rats and rats treated with the V2 receptor agonist desmopressin (dDAVP; Fig. 8*D*). Here too, AQP2 and AKAP18δ were located intracellularly in resting principal cells and mainly at the apical plasma membrane in dDAVP-stimulated cells. A quantitative evaluation of the intracellular or plasma membrane-derived epifluorescence signals in tissue sections is not possible because fluorescence signals from several layers cannot be separated. Taken together, the data point to a role of AKAP18δ in the AQP2 shuttle.

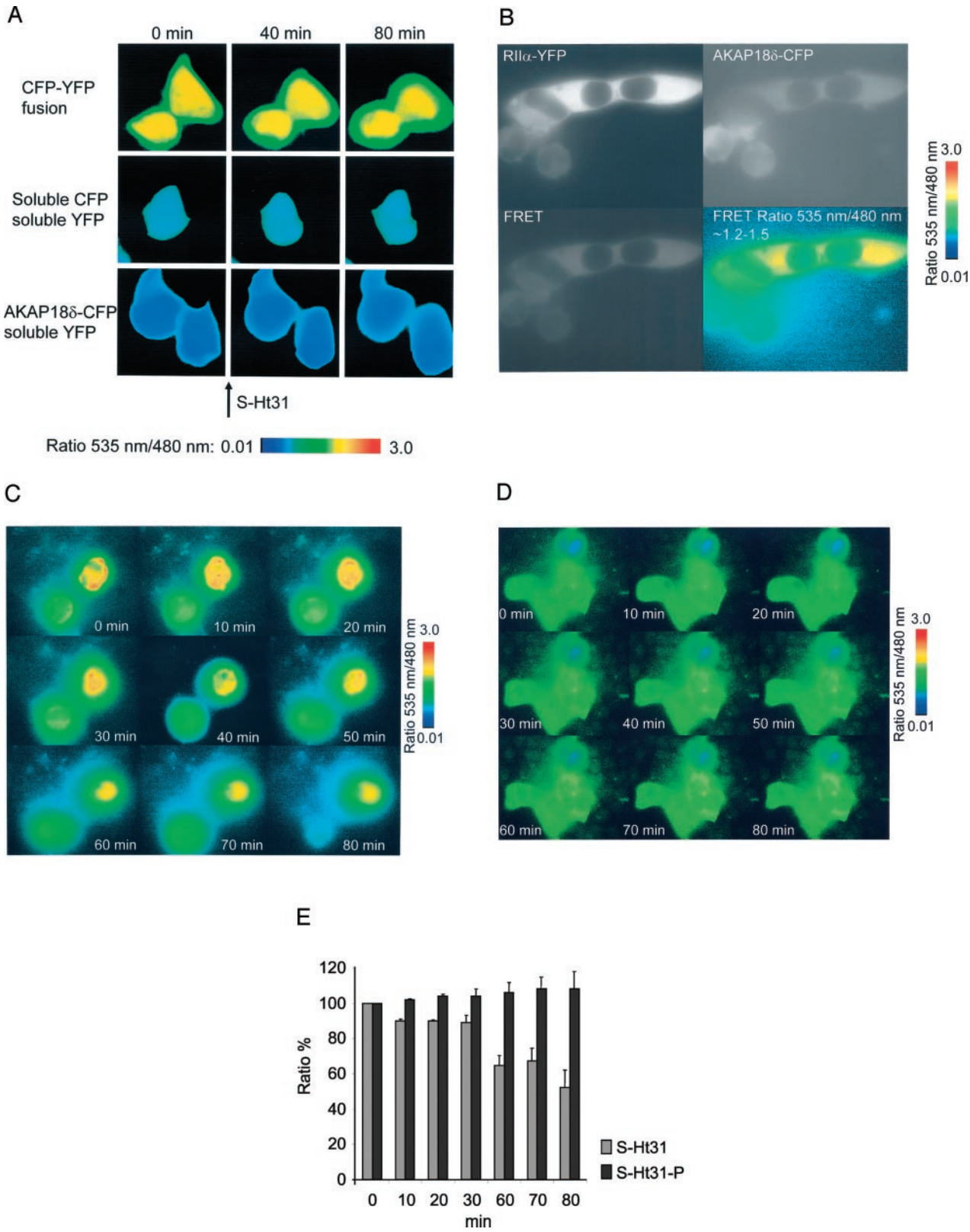

FIG. 5. **FRET measurements to visualize the interaction of AKAP18δ and regulatory RIIα subunits of PKA in living cells.** *A*, as controls, HEK293 cells were transfected with plasmids encoding a fusion of CFP and YFP (*upper panel*), co-transfected with plasmids encoding soluble CFP and YFP (*middle panel*), or with plasmids encoding AKAP18δ-CFP and soluble YFP (*lower panel*). FRET was determined prior to addition of the anchoring inhibitor peptide S-Ht31 (0 min) or 40 and 80 min thereafter. Addition of the peptide is indicated by the *arrow*. FRET is depicted as the ratio of 535/480 nm in false *colors*. *B*, HEK293 cells were co-transfected with plasmids encoding RIIα-YFP and AKAP18δ-CFP. Expression of RIIα-YFP (*upper left panel*) was detected by the fluorescence emitted by YFP after excitation at 488 nm. Expression of AKAP18δ-CFP in the same cells was detected by the fluorescence emitted by CFP after excitation at 425 nm (*upper right panel*). FRET from CFP to YFP (*lower left panel*) was determined by excitation of CFP and measurement of the fluorescence emitted from YFP (535/26 nm). The FRET ratio (535/480 nm) is depicted in false *colors*. *C* and *D*, FRET was measured in HEK293 cells co-expressing RIIα-YFP and AKAP18δ-CFP (0 min). Thereafter, the anchoring inhibitor peptide S-Ht31 (100 μM; *C*) or the control peptide S-Ht31-P (100 μM; *D*) was added and FRET was determined in 10-min intervals over a total of 80 min. *E*, quantitative evaluation of the effects of the peptides S-Ht31 and S-Ht31-P on the FRET signal from AKAP18δ-CFP to RIIα-YFP.

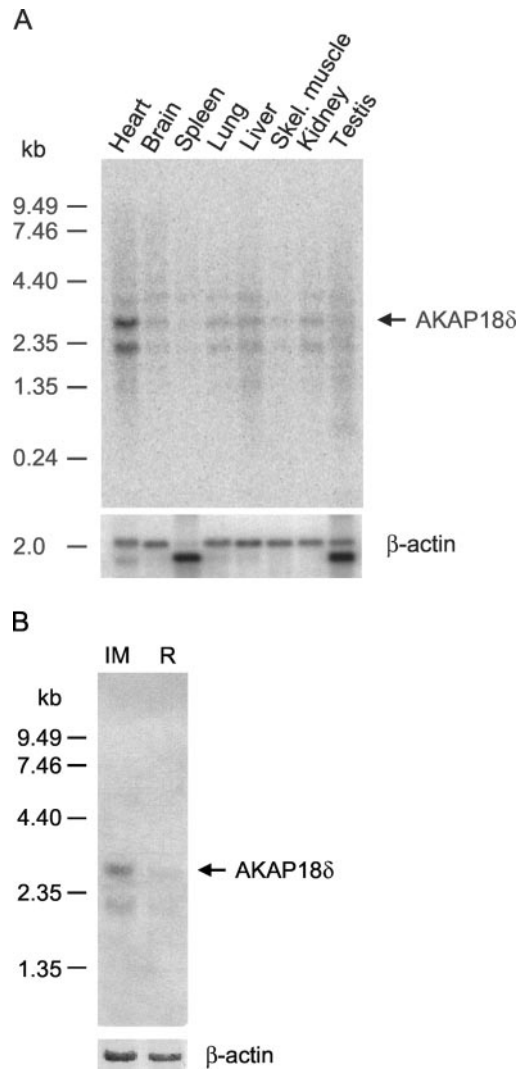

FIG. 6. **Expression pattern of AKAP18δ and other AKAP18 isoforms.** *A*, the mRNA distribution of AKAP18δ was assessed by Northern blot analysis. A multiple tissue Northern blot (tissues indicated *above* each lane) was sequentially hybridized with a radioactively labeled cDNA probe (bp 20–164 of AKAP18δ) specifically recognizing AKAP18δ and a β-actin probe. *B*, total RNA was isolated from rat renal inner medulla (*IM*) and residual kidney tissue (*R*). The RNA was separated by agarose gel electrophoresis, transferred to a nylon filter, and hybridized with a radioactively labeled cDNA probe corresponding to bp 320–1723 of AKAP18δ, which potentially hybridizes to AKAP18α, -β, -γ, and -δ. The RNA was rehybridized with a β-actin probe. Signals were visualized by autoradiography.

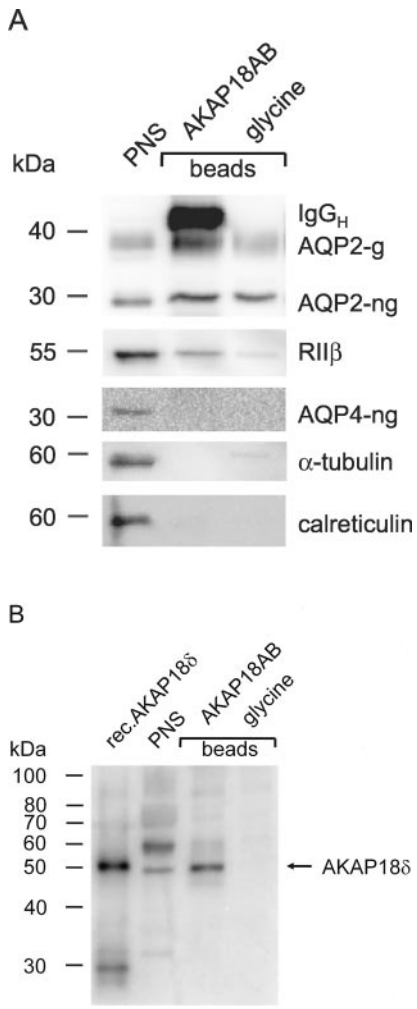

FIG. 7. **AQP2, PKA, and AKAP18δ reside on the same intracellular vesicles.** Rat renal inner medulla was homogenized and nuclei and cell debris were removed by centrifugation, resulting in the postnuclear supernatant (*PNS*). The postnuclear supernatant was incubated with affinity-purified A18δ4 antibody coupled to Eupergit C1Z methacrylate microbeads (AKAP18AB beads) or control beads (glycine beads). *A*, glycosylated (*g*) and nonglycosylated (*ng*) AQP2, regulatory RIIβ PKA subunits, and as controls, markers for the plasma membrane (nonglycosylated AQP4, *AQP4-ng*), the cytoskeleton (α-tubulin), and the endoplasmic reticulum (*calreticulin*) were detected by Western blotting. *B*, AKAPs were detected by RII overlay analysis. *rec. AKAP18δ*, recombinant AKAP18δ.

Cyclic AMP Decreases the Interaction of AKAP18δ with Regulatory PKA Subunits—To obtain further evidence for the involvement of AKAP18δ in the AQP2 shuttle, FRET experiments were carried out with a rabbit cortical collecting duct cell line stably expressing AQP2 (CD8 cells). After stimulation of CD8 cells with forskolin, a direct activator of adenylyl cyclase, AQP2 translocates to the apical plasma membrane (29, 33, 34, 56). To monitor the interaction of AKAP18δ with PKA, CD8 cells were transiently co-transfected with plasmids encoding AKAP18δ-CFP and RIIα-YFP. Excitation of CFP resulted in FRET from CFP to YFP (Fig. 9*A*, *upper panel*, 0 s), showing a direct interaction between AKAP18δ and RIIα subunits. Addition of forskolin (100 μM) reduced the FRET signal by 50% within 60 s, indicating a dissociation of the proteins. The presence of forskolin largely prevented the reassociation of AKAP18δ and RIIα as the FRET signal only increased by 15% over the following 600 s (Fig. 9, *A* and *B*). Donor recovery after acceptor bleaching was only observed in cells co-expressing AKAP18δ-CFP and RIIα-YFP (data not shown).

DISCUSSION

AVP induces a PKA-dependent redistribution of AQP2-bearing vesicles to the plasma membrane of renal principal cells. The redistribution of AQP2 is inhibited by the uncoupling of PKA from AKAPs (26). The identity of the AKAP(s) involved, however, is unknown. We have identified a new splice variant of AKAP18, AKAP18δ (Fig. 1). AKAP18δ function as an AKAP both *in vitro* and *in vivo* (Figs. 3–5). In the kidney it is enriched in the inner medulla and closely resembles the distribution of AQP2 (Figs. 6 and 8). The by far major portion of AKAP18δ is present in the soluble fraction of renal inner medullary cells (Figs. 4 and 8); within the particulate fraction AKAP18δ resides on the same intracellular vesicles as AQP2 (Fig. 7). AKAP18δ co-translocates with AQP2 to the plasma membrane upon AVP stimulation of primary cultured IMCD cells and principal cells *in situ* (Fig. 8). These findings suggest a role of AKAP18δ in the AQP2 shuttle.

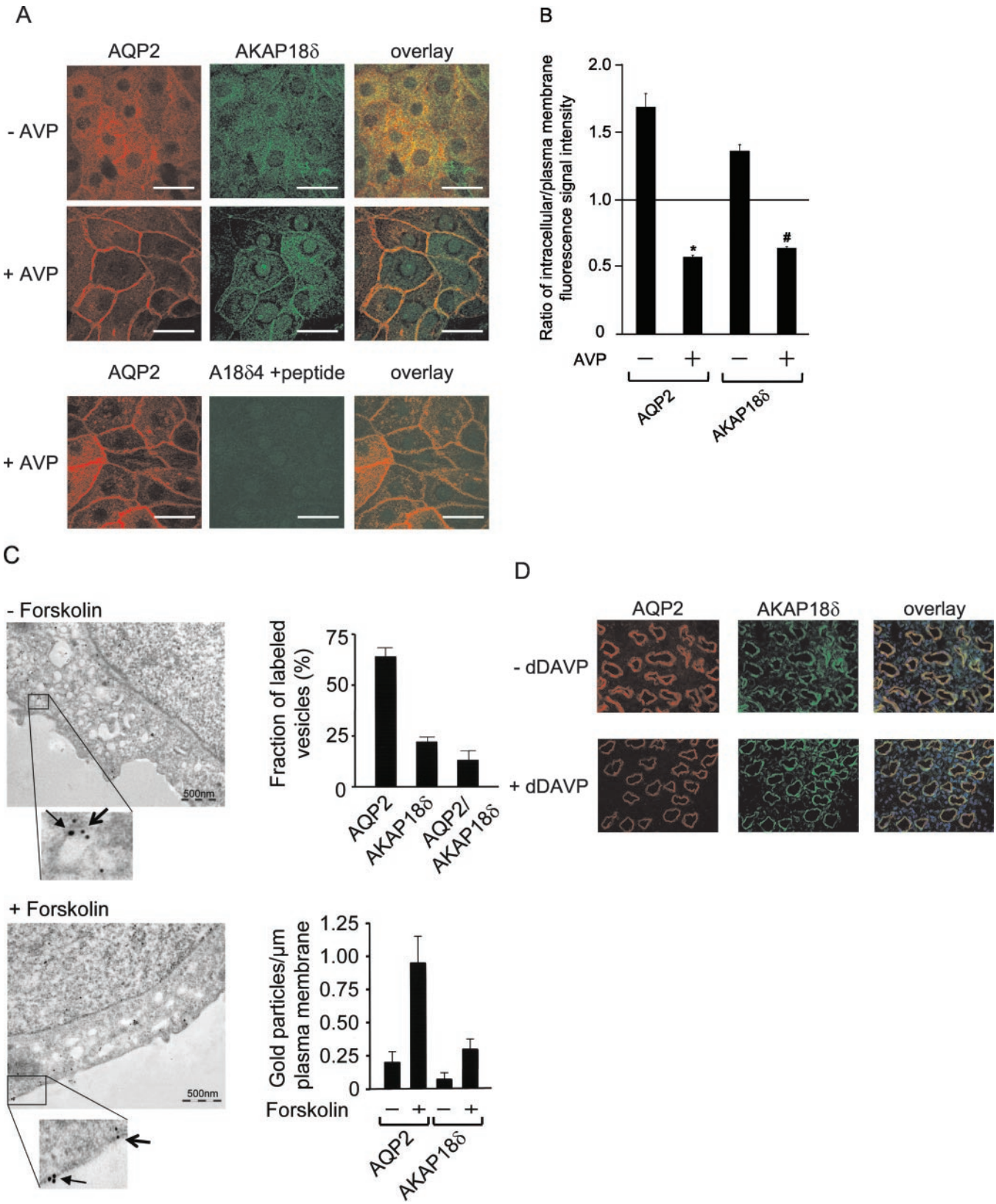

FIG. 8. *A*, the effect of AVP on the subcellular distribution of AQP2 and AKAP18δ in IMCD cells. IMCD cells were left untreated (control) or incubated with AVP (100 nM, 15 min), fixed, and permeabilized. AQP2 was detected by incubation with goat anti-AQP2 antibody and secondary Cy3-conjugated anti-goat antibodies, AKAP18δ with affinity-purified rabbit anti-AKAP18δ antibody A18δ4 and secondary Cy5-conjugated anti-rabbit antibodies. As a control, AVP-treated cells were incubated with antibody A18δ4 blocked with the peptide used for immunization (*lower panel*). Immunofluorescence signals were detected by laser scanning microscopy. The overlay of Cy3 and Cy5 fluorescence signals is shown in the *right panel*. *Scale bars*, 20 μm. *B*, quantitative analysis of the effect of AVP on the localization of AQP2 and AKAP18δ in IMCD cells. IMCD cells were treated as indicated in *A*. AQP2 and AKAP18δ immunofluorescence signals were detected by laser scanning microscopy. The intracellular and plasma membrane fluorescence signal intensities were determined and related to nuclear signal intensities. Ratios of intracellular/plasma membrane signal intensities were calculated ($n \geq 20$ cells for each condition tested; mean ± S.E.; three independent experiments). Ratios >1 indicate a mainly intracellular distribution of AQP2 and AKAP18δ, and ratios <1 indicate a predominant localization at the plasma membrane.

In addition to AKAP18δ, other proteins are associated with AQP2-bearing vesicles, for example, the motor protein dynein, the SNARE protein VAMP2, or the SNAP25-associated protein Hrs-2 (56–58). Whereas VAMP2 and dynein appear to be exclusively located on the vesicles, Hrs-2 appears to be present on both the vesicles and at the plasma membrane. VAMP2 is required for fusion of AQP2-bearing vesicles with the plasma membrane (56), and Hrs-2 may play a modulatory role in the fusion process (57). Dynein may be involved in the vesicular transport of AQP2-bearing vesicles to the plasma membrane along microtubules (58). None of these proteins co-translocates with AQP2 to the plasma membrane. In contrast, AKAP18δ translocates to the plasma membrane after elevation of cAMP. AKAP18δ may not only anchor PKA at the vesicular membrane to facilitate AQP2 phosphorylation, but may also be relevant for the transport of AQP2 to the plasma membrane. In this context it is of interest that AKAP79 is also involved in the transport of L-type Ca^{2+} channels to the plasma membrane (59).

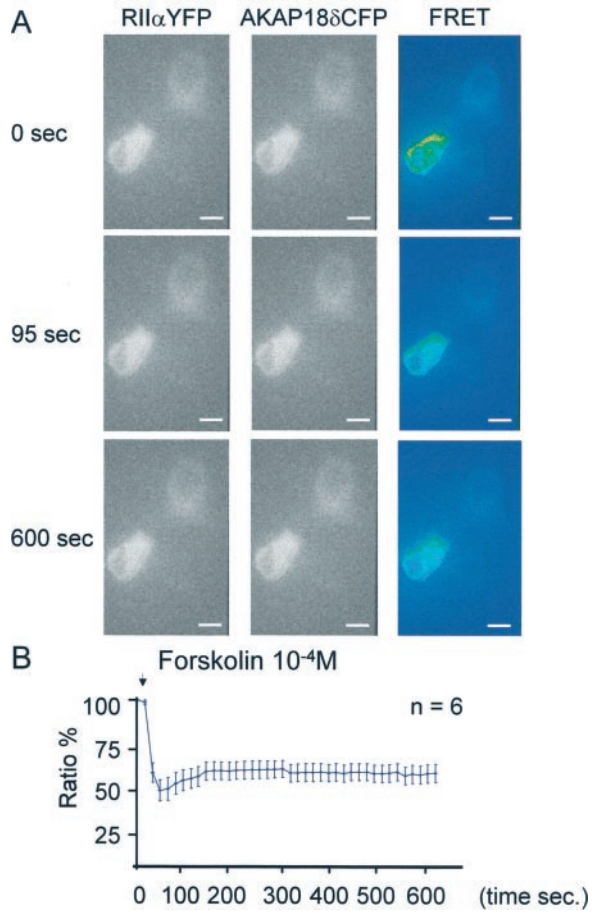

FIG. 9. **The effect of elevation of cAMP on the interaction of AKAP18δ and regulatory RIIα subunits of PKA.** *A*, CD8 cells were co-transfected with plasmids encoding RIIα-YFP and AKAP18δ-CFP. FRET was measured before and after forskolin (100 μM) was added. Shown are two representative cells co-expressing RIIα-YFP and AKAP18δ-CFP prior to forskolin addition (0 s) and 95 and 600 s thereafter (95 and 600 s). The FRET signal (ratio of 535/480 nm) is depicted in false *colors*. *B*, quantitative evaluation of the effect of forskolin on the FRET signal ($n = 6$ cells). *Scale bar*, 20 μm.

Vesicles immunoisolated from rat kidney inner medulla with antibody A18δ4 contain RIIβ subunits (Fig. 7), indicating that AKAP18δ anchors PKA type II at the vesicular membrane. RII overlay assays point to the presence of additional AKAPs on immunoisolated AQP2-bearing vesicles derived from rat renal inner medulla and primary cultured IMCD cells (data not shown), and a 90-kDa AKAP was detected on endosomes purified from rat IMCD cells (60). Thus, several AKAPs are likely to anchor PKA at AQP2-bearing vesicles. In agreement with Jo *et al.* (60), AQP2 was not detectable in cAMP-agarose precipitates obtained in the presence of detergents (data not shown), suggesting that AQP2 is not part of a protein complex formed by an AKAP.

The mechanism by which AKAP18δ associates with AQP2-bearing vesicles remains to be determined. AKAP18δ lacks the membrane targeting domain present in AKAP18α and AKAP18β (see "Introduction"), and palmitoylation was not detected (data not shown). Sequence analysis, however, suggests the presence of a myristoylation consensus site. Myristoylate, covalently bound to this site, may mediate attachment to a membranous compartment. Alternatively, AKAP18δ may bind to membranes through another, so far unknown component as was proposed for AKAP18γ (17). AKAP18α contains a leucine zipper motif mediating the interaction with L-type Ca^{2+} channels through a leucine zipper-binding motif (13). The leucine zipper motif is conserved in AKAP18δ and may be required for an interaction with a leucine zipper-binding motif-containing protein that is located on AQP2-bearing vesicles. The limited availability of an AKAP18δ-binding protein may limit the association of AKAP18δ with membranes, explaining the large portion of cytosolic AKAP18δ (Fig. 4).

AKAP18δ is a high affinity AKAP (Fig. 2). We found that the K_D for the binding of peptides derived from the RII-binding domain of AKAP18δ to RII subunits is not only determined by the core region required for RII binding (amino acid residues 301–314). Instead, the K_D increased with the length of the sequence flanking the core region (peptide array studies, data not shown). Zakhary *et al.* (61) determined the K_D for the binding of a short synthetic peptide corresponding to the RII-binding site of AKAP18α to RIIα subunits in surface plasmon resonance measurements ($K_D = 6.6$ μM). The peptides used by Zakhary *et al.* (61) lack the region flanking the RII-binding site, which may explain the discrepancy in the results.

* and #, values significantly different from untreated control cells for the detection of AQP2 and AKAP18δ, respectively ($p < 0.001$). *C*, immunogold labeling of AQP2 and AKAP18δ in control and forskolin-treated IMCD cells. IMCD cells were left untreated (−forskolin) or incubated with forskolin (100 μM, 15 min) and processed for immunogold electron microscopy as described under "Experimental Procedures." AQP2 (→) and AKAP18δ (➜) were detected by using the same primary antibodies as in *A*. As secondary antibodies donkey anti-goat IgG, labeled with 12-nm gold particles, and donkey anti-rabbit IgG, labeled with 18-nm gold particles were used (*scale bar*, 500 nm). The *upper image* was assembled from four and the lower from two separately recorded images, respectively, using analySIS software. The magnified view from the control cell (*upper image*) shows a representative vesicle containing AQP2 and AKAP18δ. The magnified view from the forskolin-treated cell (*lower image*) shows a plasma membrane region with AQP2 and AKAP18δ. *Upper right panel*, intracellular vesicles ($n = 127$) in images from control cells obtained from two independent experiments were analyzed for the presence of AQP2 and/or AKAP18δ. Shown is the percentage of vesicles containing AQP2, AKAP18δ, or both. *Error bars* indicate the deviation from the mean. *Lower right panel*, the number of gold particles/μm of plasma membrane in control and forskolin-treated IMCD cells was determined ($n = 6$ cells for each condition). *Error bars* indicate the deviation from the mean. *D*, cryo-sections from rat renal inner medulla of control and dDAVP-treated rats were incubated with affinity-purified anti-AKAP18δ antibody A18δ4 and secondary fluorescein isothiocyanate-conjugated anti-rabbit antibodies (*middle panels*) and subsequently with goat anti-AQP2 and secondary Cy3-conjugated anti-goat antibodies (*left panels*). Nuclei were stained with 4′,6-diamino-2-phenylindole. Fluorescence signals were visualized by epifluorescence microscopy (magnification ×300). The overlay of 4′,6-diamino-2-phenylindole, fluorescein isothiocyanate, and Cy3 fluorescence is shown in the *right panels*.

Surface plasmon resonance measurements show that an N-terminal truncated AKAP18δ binds RII subunits of PKA with higher affinity than the full-length protein. This observation indicates that steric hindrance by the N terminus limits the access of RII subunits to the full-length AKAP18δ (Fig. 2, Table I). Masking of the RII-binding site may constitute a regulatory mechanism for the interaction with PKA. A molecular basis for the regulation of the interaction between AKAP18δ and RII subunits is at present not known. We have not observed phosphorylation of AKAP18δ by PKA (data not shown). Thus PKA-mediated phosphorylation of AKAP18δ decreasing its affinity to RII subunits is not a likely mechanism. It remains, however, possible that other protein kinases are involved. In this context it is of interest that AKAP18δ possesses consensus sites for protein kinase C- and casein kinase 2-mediated phosphorylation. The hypothesis of a regulated interaction between AKAP18δ and RII subunits is consistent with our finding that the elevation of cAMP in CD8 cells, a cell culture model of renal principal cells, induces the dissociation of AKAP18δ and RIIα subunits of PKA (Fig. 9). The dissociation of RII subunits from AKAPs associated with the AQP2-bearing vesicle explains that AKAPs but not RII subunits co-translocate with AQP2 to the plasma membrane of principal cells (26). Functionally, the dissociation of RII subunits from AKAPs may constitute a negative feedback system: the dissociated RII subunits scavenge and thereby inhibit free catalytic subunits (3), ensuring the termination of the cAMP signal. In this context it may be relevant that AKAPδ is present throughout the cytosol (Figs. 4 and 8). Cytosolic AKAP18δ may redirect the PKA holoenzyme to its intracellular target site by binding to a membrane-attached binding protein (see above).

In the present study, the FRET technique was applied to determine the AKAP function of AKAP18δ *in vivo*. This approach, however, turned out to be rather valuable to confirm various properties ascribed to AKAP18δ by biochemical means. The FRET experiments support the view that AKAP18δ is located in the cytosol as the AKAP18δ-CFP fusion was present throughout the cytosol of HEK293 cells, and they confirm the assumed RII-binding site. In addition, they show a decreased interaction of AKAP18δ with RIIα subunits in response to cAMP elevation in principal cells. The decreased interaction of AKAP18δ and regulatory subunits was also evident in cAMP-agarose pull-down experiments: cAMP-agarose pull-downs from AVP-treated primary cultured IMCD cells contained 50% less AKAP18δ than the precipitates from control cells (data not shown). Potentially, the FRET approach allows visualization of any AKAP-PKA complex and, by using an organelle marker in conjunction with the AKAP-PKA complex, it may help to determine the subcellular site of the AKAP-PKA interaction. Indeed, Oliveria *et al.* (62) recently used the FRET technique to study the interaction of AKAP79 with RII subunits and protein phosphatase 2B at the plasma membrane. Moreover, by tagging several AKAPs with different GFP versions and the catalytic PKA subunit with a GFP version compatible for FRET measurements with the tagged AKAPs (7, 63, 64), the spatial and temporal organization of cAMP signaling can be studied with the FRET technique.

Except for renin secretion from juxtaglomerular kidney cells, the AVP-induced AQP2 translocation is the only example of an exocytic process solely triggered by cAMP (54). Some other exocytic processes such as proton secretion from gastric parietal cells may be triggered by cAMP or Ca^{2+} increases, and yet others are strictly dependent on Ca^{2+} increases and are only modulated by cAMP (for review see Ref. 19). AKAPs appear to be involved in all of these cAMP-controlled exocytic processes: AKAP18δ in the AQP2 shuttle, Ezrin in proton secretion (51), and AKAP18α in insulin secretion (8). The role of AKAPs in renin secretion has not been investigated. Dysregulation of these processes leads to diseases including congenital and acquired nephrogenic diabetes insipidus, hypertension, gastric ulcers, and diabetes mellitus. The pharmacological interference with the function of specific AKAPs may prove a suitable concept for the treatment of these diseases. With the identification of peptides selectively displacing either PKA type I or type II from the dual specificity AKAP D-AKAP2 (65) or the generation of $AKAP_{IS}$ (50), a general disruptor of PKA anchoring, prototypical agents are already at hand to modulate anchored cAMP signaling.

Acknowledgments—We thank A. Geelhaar, M. Ringling, M. Gomoll, and U. Müller for excellent technical assistance, and C. Hundsrucker and G. Krause for data base searches and molecular modeling studies. We are grateful to Dr. J. D. Scott (Howard Hughes Medical Institute, Vollum Institute, Oregon Health and Science University, Portland, OR) for providing pGST-AKAP18α, and Dr. K. Tasken (The Biotechnology Centre of Oslo, University of Oslo, Norway) for providing pGST-RIIα. We thank Dr. M. Veit (Institut für Immunologie und Molekularbiologie, Fachbereich Veterinärmedizin, Free University Berlin, Germany) for testing lipid modifications of AKAP18δ. We thank A. Oksche and M. Schaefer for helpful discussions about the FRET technique and G. Schultz for critically reading the manuscript.

REFERENCES

1. Skalhegg, B. S., and Tasken, K. (2000) *Front. Biosci.* **5,** D678–693
2. Johnson, D. A., Akamine, P., Radzio-Andzelm, E., Madhusudan, M., and Taylor, S. S. (2001) *Chem. Rev.* **101,** 2243–2270
3. Francis, S. H., Poteet-Smith, C., Busch, J. L., Richie-Jannetta, R., and Corbin, J. D. (2002) *Front. Biosci.* **7,** D580–592
4. Colledge, M., and Scott, J. D. (1999) *Trends Cell Biol.* **9,** 216–221
5. Smith, F. D., and Scott, J. D. (2002) *Curr. Biol.* **12,** R32–R40
6. Tasken, K., and Aandaal, E. M. (2004) *Physiol. Rev.* **84,** 137–167
7. Zaccolo, M., and Pozzan, T. (2002) *Science* **295,** 1711–1715
8. Fraser, I. D., Tavalin, S. J., Lester, L. B., Langeberg, L. K., Westphal, A. M., Dean, R. A., Marrion, N. V., and Scott, J. D. (1998) *EMBO J.* **17,** 2261–2272
9. Gray, P. C., Tibbs, V. C., Catterall, W. A., and Murphy, B. J. (1997) *J. Biol. Chem.* **272,** 6297–6302
10. Gray, P. C., Johnson, B. D., Westenbroek, R. E., Hays, L. G., Yates, J. R., 3rd, Scheuer, T., Catterall, W. A., and Murphy, B. J. (1998) *Neuron* **20,** 1017–1026
11. Gray, P. C., Scott, J. D., and Catterall, W. A. (1998) *Curr. Opin. Neurobiol.* **8,** 330–334
12. Catterall, W. A. (2000) *Annu. Rev. Cell Dev. Biol.* **16,** 521–555
13. Hulme, J. T., Ahn, M., Hauschka, S. D., Scheuer, T., and Catterall, W. A. (2002) *J. Biol. Chem.* **277,** 4079–4087
14. Hulme, J. T., Lin, T. W., Westenbroek, R. E., Scheuer, T., and Catterall, W. A. (2003) *Proc. Natl. Acad. Sci. U. S. A.* **100,** 13093–13098
15. Tibbs, V. C., Gray, P. C., Catterall, W. A., and Murphy, B. J. (1998) *J. Biol. Chem.* **273,** 25783–25788
16. Cantrell, A., Tibbs, V., Yu, F., Murphy, B., Sharp, E., Qu, Y., Catterall, W., and Scheuer, T. (2002) *Mol. Cell Neurosci.* **21,** 63–80
17. Trotter, K. W., Fraser, I. D., Scott, G. K., Stutts, M. J., Scott, J. D., and Milgram, S. L. (1999) *J. Cell Biol.* **147,** 1481–1492
18. Brown, R. L., August, S. L., Williams, C. J., and Moss, S. B. (2003) *Biochem. Biophys. Res. Commun.* **306,** 394–401
19. Klussmann, E., Maric, K., and Rosenthal, W. (2000) *Rev. Physiol. Biochem. Pharmacol.* **141,** 33–95
20. Agre, P., King, L. S., Yasui, M., Guggino, W. B., Ottersen, O. P., Fujiyoshi, Y., Engel, A., and Nielsen, S. (2002) *J. Physiol.* **542,** 3–16
21. Nielsen, S., Frokiaer, J., Marples, D., Kwon, T. H., Agre, P., and Knepper, M. A. (2002) *Physiol. Rev.* **82,** 205–244
22. Morello, J. P., and Bichet, D. G. (2001) *Annu. Rev. Physiol.* **63,** 607–630
23. Nishimoto, G., Zelenina, M., Li, D., Yasui, M., Aperia, A., Nielsen, S., and Nairn, A. C. (1999) *Am. J. Physiol.* **276,** F254–F259
24. Fushimi, K., Sasaki, S., and Marumo, F. (1997) *J. Biol. Chem.* **272,** 14800–14804
25. Katsura, T., Gustafson, C. E., Ausiello, D. A., and Brown, D. (1997) *Am. J. Physiol.* **272,** F816–F822
26. Klussmann, E., Maric, K., Wiesner, B., Beyermann, M., and Rosenthal, W. (1999) *J. Biol. Chem.* **274,** 4934–4938
27. van Balkom, B. W., Savelkoul, P. J., Markovich, D., Hofman, E., Nielsen, S., van der Sluijs, P., and Deen, P. M. (2002) *J. Biol. Chem.* **277,** 41473–41479
28. Kamsteeg, E. J., Heijnen, I., van Os, C. H., and Deen, P. M. (2000) *J. Cell Biol.* **151,** 919–930
29. Procino, G., Carmosino, M., Marin, O., Brunati, A. M., Contri, A., Pinna, L. A., Mannucci, R., Nielsen, S., Kwon, T. H., Svelto, M., and Valenti, G. (2003) *FASEB J.* **17,** 1886–1888
30. Kuwahara, M., Fushimi, K., Terada, Y., Bai, L., Marumo, F., and Sasaki, S. (1995) *J. Biol. Chem.* **270,** 10384–10387
31. Lande, M. B., Jo, I., Zeidel, M. L., Somers, M., and Harris, H. W. (1996) *J. Biol. Chem.* **271,** 5552–5557
32. Klussmann, E., Tamma, G., Lorenz, D., Wiesner, B., Maric, K., Hofmann, F., Aktories, K., Valenti, G., and Rosenthal, W. (2001) *J. Biol. Chem.* **276,**

20451–20457
33. Tamma, G., Klussmann, E., Maric, K., Aktories, K., Svelto, M., Rosenthal, W., and Valenti, G. (2001) *Am. J. Physiol.* **281,** F1092–F1101
34. Valenti, G., Frigeri, A., Ronco, P. M., D'Ettorre, C., and Svelto, M. (1996) *J. Biol. Chem.* **271,** 24365–24370; Correction (1997) *J. Biol. Chem.* **272,** 26794
35. Tamma, G., Wiesner, B., Furkert, J., Oksche, A., Schaefer, M., Valenti, G., Rosenthal, W., and Klussmann, E. (2003) *J. Cell Sci.* **116,** 3285–3294
36. Tamma, G., Klussmann, E., Procino, G., Svelto, M., Rosenthal, W., and Valenti, G. (2003) *J. Cell Sci.* **116,** 1519–1525
37. Lu, H., Sun, T. X., Bouley, R., Blackburn, K., McLaughlin, M., and Brown, D. (2004) *Am. J. Physiol.* **286,** F233–F243
38. Maric, K., Oksche, A., and Rosenthal, W. (1998) *Am. J. Physiol.* **275,** F796–F801
39. Klussmann, E., and Rosenthal, W. (2001) *Kidney Int.* **60,** 446–449
40. Bregman, D. B., Bhattacharyya, N., and Rubin, C. S. (1989) *J. Biol. Chem.* **264,** 4648–4656
41. Herberg, F. W., Maleszka, A., Eide, T., Vossebein, L., and Tasken, K. (2000) *J. Mol. Biol.* **298,** 329–339
42. Lenz, J. C., Reusch, H. P., Albrecht, N., Schultz, G., and Schaefer, M. (2002) *J. Cell Biol.* **159,** 291–302
43. Sambrook, J., and Russel, D. W. (2001) *Molecular Cloning: A Laboratory Manual*, 3rd Ed., Cold Spring Harbor Laboratory Press, Cold Spring Harbor, NY
44. Liebenhoff, U., and Rosenthal, W. (1995) *FEBS Lett.* **365,** 209–213
45. Wang, L., Sunahara, R. K., Krumins, A., Perkins, G., Crochiere, M. L., Mackey, M., Bell, S., Ellisman, M. H., and Taylor, S. S. (2001) *Proc. Natl. Acad. Sci. U. S. A.* **98,** 3220–3225
46. Holroyd, C., Kistner, U., Annaert, W., and Jahn, R. (1999) *Mol. Biol. Cell* **10,** 3035–3044
47. Storm, R., Klussmann, E., Geelhaar, A., Rosenthal, W., and Maric, K. (2003) *Am. J. Physiol.* **284,** F189–F198
48. Kozak, M. (1996) *Mamm. Genome* **7,** 563–574
49. Carr, D. W., Hausken, Z. E., Fraser, I. D., Stofko-Hahn, R. E., and Scott, J. D. (1992) *J. Biol. Chem.* **267,** 13376–13382
50. Alto, N. M., Soderling, S. H., Hoshi, N., Langeberg, L. K., Fayos, R., Jennings, P. A., and Scott, J. D. (2003) *Proc. Natl. Acad. Sci. U. S. A.* **100,** 4445–4450
51. Dansfield, D. T., Bradford, A. J., Smith, J., Martin, M., Roy, C., Mangeat, P. H., and Goldenring, J. R. (1997) *EMBO J.* **16,** 35–43
52. Hausken, Z. E., Coghlan, V. M., and Scott, J. D. (1998) *Methods Mol. Biol.* **88,** 47–64
53. Maric, K, Wiesner, B., Lorenz, D., Klussmann, E., Betz, T., and Rosenthal, W. (2001) *Biophys. J.* **80,** 1783–1790
54. Lorenz, D., Krylov, A., Hahm, D., Hagen, V., Rosenthal, W., Pohl, P., and Maric, K. (2003) *EMBO Rep.* **4,** 88–93
55. Jo, I., Nielsen, S., and Harris, H. W. (1997) *Biochim. Biophys. Acta* **1324,** 91–101
56. Gouraud, S., Laera, A., Calamita, G., Carmosino, M., Procino, G., Rossetto, O., Mannucci, R., Rosenthal, W., Svelto, M., and Valenti, G. (2002) *J. Cell Sci.* **115,** 3667–3674
57. Shukla, A., Hager, H., Corydon, T. J., Bean, A. J., Dahl, R., Vajda, Z., Li, H., Hoffmann, H. J., and Nielsen, S. (2001) *Am. J. Physiol.* **281,** F546–F556
58. Marples, D., Schroer, T. A., Ahrens, N., Taylor, A., Knepper, M. A., and Nielsen, S. (1998) *Am. J. Physiol.* **274,** F384–F394
59. Altier, C., Dubel, S. J., Barrere, C., Jarvis, S. E., Stotz, S. C., Spaetgens, R. L., Scott, J. D., Cornet, V., De Waard, M., Zamponi, G. W., Nargeot, J., and Bourinet, E. (2002) *J. Biol. Chem.* **277,** 33598–33603
60. Jo, I., Ward, D. T., Baum, M. A., Scott, J. D., Coghlan, V. M., Hammond, T. G., and Harris, H. W. (2001) *Am. J. Physiol.* **281,** F958–F965
61. Zakhary, D. R., Fink, M. A., Ruehr, M. L., and Bond, M. (2000) *J. Biol. Chem.* **275,** 41389–41395
62. Oliveria, S. F., Gomez, L. L., and Dell'Acqua, M. L. (2003) *J. Cell Biol.* **160,** 101–112
63. Zaccolo, M., De Giorgi, F., Cho, C. Y., Feng, L., Knapp, T., Negulescu, P. A., Taylor, S. S., Tsien, R. Y., and Pozzan, T. (2000) *Nat. Cell Biol.* **2,** 25–29
64. Zhang, J., Campbell, R. E., Ting, A. Y., and Tsien, R. Y. (2002) *Nat. Rev. Mol. Cell Biol.* **3,** 906–918
65. Burns-Hamuro, L. L., Ma, Y., Kammerer, S., Reineke, U., Self, C., Cook, C., Olson, G. L., Cantor, C. R., Braun, A., and Taylor, S. S. (2003) *Proc. Natl. Acad. Sci. U. S. A.* **100,** 4072–4077